General continuum theory for multiion channel

II. Application to acetylcholine channel

David G. Levitt
Department of Physiology, University of Minnesota, Minneapolis, Minnesota 55455 USA

ABSTRACT The general theory (Levitt, D. G. 1990. *Biophys. J.* 59:271–277) is applied to a model channel that resembles the acetylcholine receptor channel (ACH). The model incorporates the known features of the ACH geometry and fixed charge locations. The channel has a wide mouth facing the outer solution, tapering to a narrow region facing the interior of the cell. Rings of fixed negative charge are placed at the two surfaces where the bilayer begins, corresponding to the known charges at the ends of the M2 segment. It is assumed that the forces acting on the ion are electrostatic: ion–channel wall, ion–ion, Born image and applied voltage. Analytical expressions for these forces are derived that take account of the low dielectric lipid region. In addition, there is a local hard sphere repulsive force that prevents ions from piling up on each other in regions of the channel with a high fixed charge density. A classical continuum theory is used to obtain an expression for the diffusion coefficient in the channel. The model can mimic the major qualitative and, in many cases, quantitative experimental features of the ACH channel: current–voltage relation, conductance versus concentration and interaction between monovalent and divalent ions. The model calculations were also compared with the site directed mutagenesis experiments of Imoto, K., C. Busch, B. Sakmann, M. Mishina, T. Konno, J. Nakai, H. Bujo, Y. Mori, K. Fukuda, and S. Numa. (1988. *Nature (Lond.)*. 335:645–648) in which the charge at the ends of the channel was systematically varied.

INTRODUCTION

An extension of the Nernst–Planck continuum equation to a general multiion channel has recently been described (Levitt, 1990). The purpose of this paper is to provide a specific example of the use of this theory by applying it to the acetylcholine receptor channel (ACH). The theory relates the channel flux to two functions that characterize the channel: $\Phi_w(x)$, the interaction potential between the ion and the channel wall; and $A(x)$, the cross-sectional area of the channel. The ACH receptor is the only biological channel in which one can make some reasonable guesses about these functions. The general outline of its shape is known and there is suggestive evidence about the location of the fixed wall charges. The most important advantage of the ACH channel is that the conductance is determined primarily by the ion's valence. For example, the relative conductance of the different monovalent cations is close (but not identical) to their bulk diffusion coefficients and, although divalent cations have a much lower conductance than monovalent cations, there is little discrimination among the divalents (Hille, 1984). This suggests that continuum diffusion effects dominate the kinetics and, as a first approximation, Φ_w can be approximated by the relatively simple long-range electrostatic potential.

A basic assumption of this paper will be that the long-range forces on the ion result only from the fixed charges in the channel. It is assumed, for example, that the dipole potentials are of short range and tend to cancel out at long range. This assumption is not in agreement with two recent papers which estimated the forces in the ACH channel based on specific assumptions about the channel protein structure and found that the dipoles could produce significant long range effects (Eisenman et al., 1990; Fourois-Corbin and Pullman, 1988). Given the present limited knowledge about the ACH channel structure, the question of the relative importance of fixed charge versus dipole potentials cannot be settled. I would hope that, even if the dipole potentials were important, the solution described here would still be useful because one could find equivalent fixed charges that could mimic the dipole potentials.

Because the model of the ACH channel that is used here is only a crude approximation to the real channel, there is no reason to carefully adjust the parameters in an attempt to get a perfect fit to the experimental channel flux. However, one would hope that the model could mimic the major qualitative features of the channel, and three specific aspects will be examined: (*a*) the interaction between monovalent and divalent cations.

Address correspondence to David Levitt, Department of Physiology, 6-255 Millard Hall, University of Minnesota, Minneapolis, MN 55455.

0006-3495/91/02/278/11 $2.00

Because the model is primarily electrostatic, this interaction represents the best probe of this potential. (*b*) The current–voltage (I–V) relationship. The ACH channel has a relatively linear I–V curve. Because this seems to be a characteristic property of most biological channels, one would hope that it would also be a relatively robust property of the model. (*c*) The conductance versus concentration relationship. Saturation of the conductance at high concentrations (usually near the physiological range) is another characteristic feature of biological channels.

DESCRIPTION OF CHANNEL MODEL

Structure of channel

A schematic diagram of the model is shown in Fig. 1. It shows the portion of the channel that spans the bilayer region of the membrane and is based on the structure described in the review by Dani (1989*b*). The narrow end of the channel is at the intracellular side of the membrane. A distinction must be made between the electrostatic and the physical structure. The electrostatic structure describes the hypothetical region where there is a transition between the high dielectric aqueous region and the low dielectric lipid region. It is the structure that determines the magnitude of the electrostatic potential. The solid lines in Fig. 1 indicate this electrostatic structure. As shown in Fig. 1, it is assumed that the regions of the channel that project into the bulk solution have a high dielectric constant (equivalent to water). The physical structure of the channel (Fig. 1, *dashed line*) should be smaller than the electrostatic structure of the channel because the inner region of the channel is polar and has a relatively high dielectric constant. The physical structure extends beyond the bilayer at the narrow end by an (variable) amount G_1. Although the physical channel extends far beyond the bilayer at the external side, it will be assumed that it has such a large diameter in this region that it is not rate limiting and can be approximated by bulk solution.

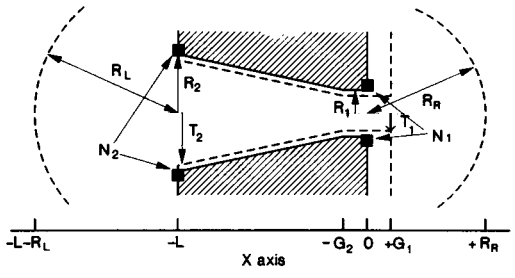

FIGURE 1 Cross-section through the model of the ACH channel. The solid lines outline the electrostatic channel and the dashed lines outline the physical channel. The narrow end of the channel faces the cell interior. The solid squares indicate sections through the ring of fixed charge of valence N_1 and N_2. The channel is drawn to scale for the following dimensions (in angstroms): lipid thickness (L = 32); electrostatic radius at narrow and wide end (R_1 = 4; R_2 = 10); physical radius at narrow and wide end (T_1 = 3; T_2 = 9); length of narrow electrostatic region (G_2 = 4); length of extension of narrow region beyond electrostatic region (G_1 = 4).

The general solution (Levitt, 1990) allows for an arbitrary number of axially symmetric rings of fixed charges, placed at arbitrary positions in the channel. Results will be described for the case where charges of valence N_1 and N_2 are placed at the narrow and wide ends of the (electrostatic) channel (Fig. 1), corresponding to the known charged regions at the ends of the M2 helix (Imoto et al., 1988). The narrow region with its fixed charge should have the properties that are usually assigned to an "ion binding site." The ACH channel probably has more than two rings of charge and some rings may be located in regions of the channel which are external to the bilayer. The basic assumption used to solve the electrostatic equations (perpendicular component of the E field is zero at the channel wall) limits the locations of the charge to regions within the bilayer. It is hoped that by adjusting the charge N_2 in Fig. 1, it should be possible to mimic the real channel.

The channel is characterized by the following additional parameters: L, the thickness of the low dielectric lipid region; R_1 and R_2, the electrostatic radius of the narrow and wide ends; T_1 and T_2, the physical radius of the narrow and wide ends; G_2, the length of the narrow electrostatic region of constant radius; $G_2 + G_1$, the length of the narrow physical region; R_L and R_R, the radial distance from the channel ends where the analytical boundary condition is used (Levitt, 1990). The parameters are all normalized by dividing by R_1. Changes in just R_1 produce changes in the scale of the channel, leaving the shape unchanged. The following set of parameters (in angstroms) were used for all of the results described in this paper: R_1 = 4, R_2 = 10, L = 32, T_1 = 3, T_2 = 9, $G_2 = G_1$ = 4, R_L = 24, R_R = 20. The position of the fixed charges (N = O to −2) is at $X = -L$ (the left end) and X = 0 (the right end). Thus, the electrostatic channel was 32 Å long and the numerical region included 24 and 20 Å of bulk solution at the left and right end, respectively. Fig. 1 is drawn to scale for these dimensions.

Electrostatic potentials

Analytical expressions for the electrostatic potentials were derived using the assumption that the perpendicu-

lar component of the E field at the electrostatic boundary is zero. It is assumed that there is some prescribed surface at each axial position on which the fields (and all other channel properties) are constant. This means that the system is described by just one spatial parameter (X), the position along the axis. The potentials depend on what form is assumed for the constant E surface, and once this form is chosen, the analytical potentials can be easily derived. This surface and the details of the derivation of the ion–wall, ion–ion, Born and applied potential are described in the Appendix (see Fig. 11). The use and validity of these assumption have been discussed previously (Levitt, 1985, 1987).

These expressions are clearly only crude approximations, especially in the wide regions of the channel where the true potentials should be three dimensional. They are used with the hope that the channel kinetics will not depend on the exact details of these potentials. The electrostatic radius should be regarded as an adjustable parameter, characterizing the strength of all the electrostatic fields. Fig. 2 shows the variation with position of the fixed charge, Born and applied potential for charges of -2 at both ends of the bilayer region of the channel ($X = -32$ and 0 Å) for a channel with the specific dimensions listed above.

Restricted ion area

The cross-sectional area that is available to the ith ion (A_i) is equal to πZ^2, where Z is equal to the physical radius minus the radius of the ith ion (see Appendix, Fig. 11). The details of the definitions of this area for the hemispherical surfaces at the channel ends are described in the Appendix. For all the results reported here, it is assumed that all the ions have a radius of 1.5 Å. This area [$A_i(X)$] relative to the area at the left end of the channel ($X_L = -32$ Å) is plotted in Fig. 2 for a channel with the dimensions listed above.

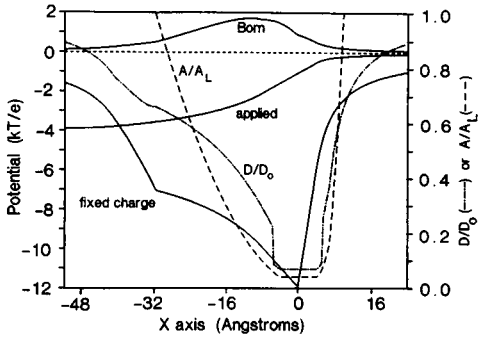

FIGURE 2 Profile of fixed charge, Born and applied electrostatic potential (100 mV, inside positive) for a channel with the dimensions of Fig. 1 and fixed charges of -2 at both ends (*solid lines*). Also shown is the continuum diffusion coefficient relative to the bulk value (D/D_o) and the physical area (A) available to the center of an ion of radius 1.5 Å normalized by the area at the left end ($A_L, X = -32$ Å).

Diffusion coefficient

The expression which is needed in the theory is the ratio $D(X)/D_o$, the diffusion coefficient at X relative to the bulk aqueous value. As a first approximation, this ratio was approximated by the continuum expression for an infinite uniform cylinder that had a radius equal to the local physical radius at X (see Appendix). In the narrow region of the channel, this ratio was reduced by an additional factor (=0.4) to take account of the "single-file" effects that are expected in this region (Dani, 1989*a*). This function is plotted in Fig. 2. The diffusion coefficient in this narrow region has an important effect on the channel kinetics because it determines when this region becomes rate-limiting. Adding the "single-file" factor of 0.4 reduces the conductance by ~30%. Again, these expressions for the diffusion coefficient are crude approximations that are probably best regarded as adjustable parameters. In the following calculations it will be assumed that the bulk diffusion coefficient (D_o) is 2×10^{-5} and 1×10^{-5} cm^2/s for monovalents and divalents, respectively.

Hard sphere radius

A critical feature of the model is the assumption that at each position in the channel there is a volume that can contain at most one ion (referred to as the "one-ion region") which is determined by the hard sphere radius (R_{HS}) of the ion. This introduces a strong ion–ion interaction and prevents ions from piling up on top of each other in regions of the channel that have a large fixed wall charge. Results will be shown only for the case where R_{HS} is equal to twice the ion radius, corresponding to the distance of closest approach when two ions are touching each other. The results did not have a strong dependence on this radius, and, for example, increasing this radius by a factor of two did not change the qualitative behavior. In the narrow region of the channel (Fig. 1) the ions cannot pass each other and it was assumed that the one-ion region was equal to the total channel volume within an axial distance of $\pm R_{HS}$. In the wider regions of the channel it was assumed that the one-ion region was a sphere of radius R_{HS}. See Appendix for more details.

Numerical solution

The general solution for this model has been described in the previous paper (Levitt, 1990) and some additional

details are listed in the Appendix. The solution was found at 228 equal intervals along the x-axis (each interval corresponds to 0.33 Å). The solution is obtained iteratively and the criteria for stopping the iteration was that the estimated value of the flux for the next iteration differed from the previous estimate by $<10^{-3}$. This usually required ~ 20 iterations and took ~ 1 min on an IBM type 25 mHz microcomputer. The program was written in Pascal and is available upon request.

RESULTS

Monovalent cation conductance versus concentration

Fig. 3 shows the concentration dependence of the conductance at an applied voltage of -100 mV (inside negative) for a channel with a fixed charge of $N_2 = -2$ at the wide end and a fixed charge at the narrow (intracellular) end (N_1) varying from 0 to -2.5 with symmetrical monovalent solutions. Except for the case where $N_1 = 0$, the conductance is due almost entirely to the flux of the cation, with the anion flux varying from 10^{-4} of the total flux for $N_1 = -1$ to 10^{-10} for $N_1 = -2.5$. When $N_1 = 0$, the cation selectivity results from the charge at the wide end and there is a much weaker charge discrimination, with an anion flux that is $\sim 10\%$ of the total flux. Fig. 4 shows a similar set of curves for a fixed charge at the narrow end of -2 and the fixed charge at the wide end varying from 0 to -2.

Increasing the fixed negative charge at the wide pore end increases the conductance, which is expected because the negative charge should increase the cation concentration at the pore mouth. In contrast, the conductance at high concentrations has a complicated dependence on the fixed charge at the narrow end: increasing when the charge is raised from 0 to -1, then decreasing as the charge is increased to -1.5 to -2 and then increasing again as the charge is raised to -2.5. This complicated behavior can be explained qualitatively by the following three competing effects. (*a*) At low values of the fixed charge (<-1), increasing the charge increases the concentration in the fixed charge region, which increases the conductance. (*b*) Increasing the charge above one leads to only a small increase in concentration (because the hard sphere repulsive potential allows at most one ion in this region) but to a large increase in the energy well, decreasing the conductance. (*c*) As the charge increases above two, the screening of the charge by the one monovalent cation at the charged site becomes relatively smaller, and the other cations attracted to this position displace the bound ion, increasing the conductance.

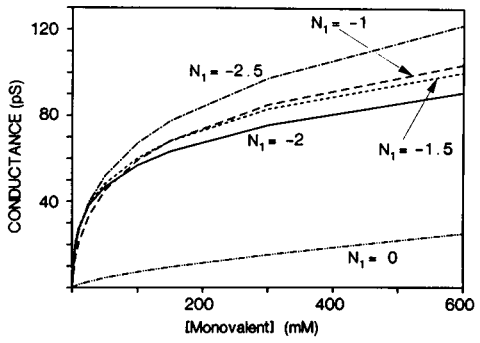

FIGURE 3 Monovalent ion conductance as a function of concentration for symmetric solutions of pure monovalent cation and anion at an applied voltage of -100 mV (inside negative). The channel has a fixed charge (N_2) at the wide end of -2 and a fixed charge at the narrow end (N_1) varying from 0 to -2.5, with the rest of the parameters given in Fig. 1.

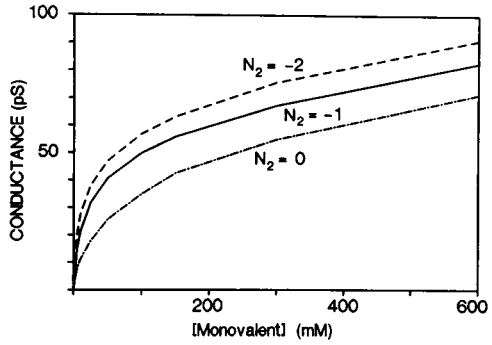

FIGURE 4 Same as Fig. 3 except that N_1 is fixed at -2 and N_2 varies from 0 to -2.

Current versus voltage

Fig. 5 shows the I–V curve for a fixed charge at the wide end of -2 and a fixed charge at the narrow end of -1 or

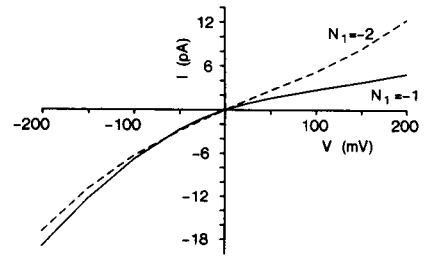

FIGURE 5 Current (I) versus voltage (V) curve for symmetrical monovalent 150-mM solutions. The fixed charge at the wide end (N_2) is -2 and the fixed charge at the narrow end is -1 (——) or -2 (- - -).

-2 (in symmetrical 150 mM monovalent). The curve for $N_1 = -2$ is relatively linear, typical of what is seen for many biological channels. For $N_1 = -1$, there is a larger asymmetry, with the conductance for inward currents significantly larger than for outward currents.

Interaction between monovalent and divalent cations

The inset in Figs. 6 and 7 shows the decrease in conductance (at an applied voltage of -100 mV, inside negative) when divalent cations are added to the external solution with 150 mM monovalent on both sides. The magnitude of the divalent block of conductance has a very strong dependence on the fixed charge (N_1) at the narrow channel end. When $N_1 = -1.3$, there is a 50% block when the divalent concentration is ~16 mM (Fig. 6). When $N_1 = -2.3$, only 0.35 mM divalent will produce a 50% block (Fig. 7). Figs. 6 and 7 also show the I–V curves in the presence of external divalent cations. As expected, at high positive voltages (outward currents) the block is relieved. The flux of the divalent is much less than that of the monovalent. For $N_1 = -1.3$ and a divalent concentration of 16 mM, the divalent flux is 2.4% of the total flux. For $N_1 = -2.3$ and a divalent concentration of 0.4 mM, the divalent flux is 0.03% of the total flux.

Influence of pore geometry

Table 1 and 2, show the effects of varying two different aspects of the pore geometry. In Table 1, the electrostatic radius of the narrow region (Fig. 1, R_1) was varied, with $N_1 = -1.5$, $N_2 = -2$, and all other variables fixed at

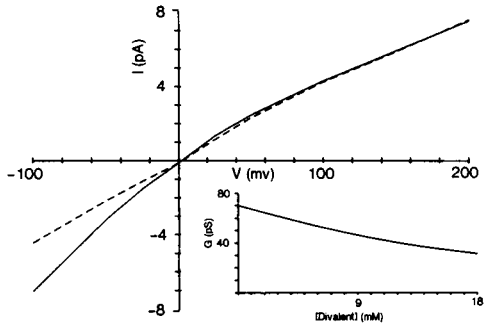

FIGURE 6 Current voltage relation for solution of 150 mM monovalent on both sides, with (- - -) or without (——) the addition of 10 mM divalent on outside for $N_1 = -1.3$ and $N_2 = -2$. The inset shows the conductance at varying concentrations or external divalent at an applied voltage of -100 mV. Addition of divalent produces a slight shift in the reversal potential that cannot be seen at the scale of this figure.

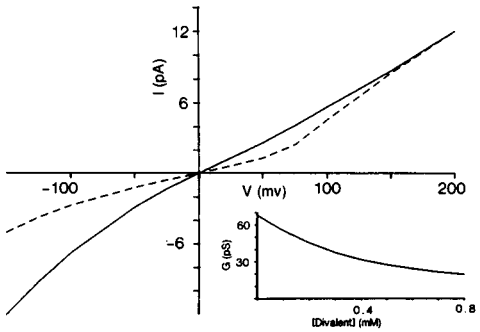

FIGURE 7 Same as Fig. 6 but with $N_1 = -2.3$ and $N_2 = -2$.

the conditions listed in Fig. 1. Decreasing this radius from 4 to 2.67 Å, decreased the conductance by >fourfold. Increasing the radius from 4 to 6 Å increased the conductance by ~60%, whereas a further increase to 8 Å leads to a slight decrease in conductance. This bimodal result is presumably due to a competition between the same three effects that were observed when the fixed charge was varied (see above). Decreasing the electrostatic radius, results in an increase in the electrostatic potential because the field lines are constrained to a smaller cross-sectional area. However, this increase differs qualitatively from that produced by simply increasing the fixed charge. For example, consider the case where the fixed charge is -1 and the potential is increased by reducing the electrostatic radius. The presence of one monovalent cation at the charged site will completely screen the fixed charge, for any electrostatic radius. In contrast, if the potential is increased by increasing the fixed charge, the presence of one ion at the charged site will only partially screen the fixed charge.

Table 2 shows the influence of the length of the narrow region G_2 (Fig. 1) on the conductance. Increasing this length, increases the diffusional resistance in this region and increases the effective electrostatic potential. Both of these effects lead to the ~50% decrease in conductance when the length is increased from 4 to 8 Å.

TABLE 1 Conductance (pS) as a function of the radius (angstroms) of the electrostatic channel

Radius	Conductance
2.67	14.6
4.0	68.2
6.0	106.2
8.0	81.6

TABLE 2 **Conductance (pS) as a function of length (angstroms) of narrow electrostatic region**

Length	Conductance
0.0	84.2
2.0	81.6
4.0	68.2
6.0	51.5
8.0	39.3

Equivalent free energy profile

The final expression for the flux of ion i (j_i) can be written in a very simple form (see Levitt, 1990; Eq. 7):

$$j = (c_{i1}e^{z_i\gamma v_1} - c_{i2}e^{z_i\gamma v_2})/h_i(\infty)$$

$$h_i(x) = \int_{-\infty}^{x} g(\alpha)\,d\alpha \quad g(\alpha) = \frac{e^{z_i\gamma u_i}}{a_i d_i} \quad \gamma = \frac{e^2}{kT\epsilon_w R}, \qquad (1)$$

where $u_i(x)$ is the total potential acting on the ion at x, including the diffuse and hard sphere ion–ion interactions along with the ion–wall potential. The term $a_i(x)$ is the cross-sectional area available to the ion, $d_i(x)$ is the diffusion coefficient, c_{1i} and c_{2i} are the bulk concentrations on the two sides, and γ is a constant. Eq. 1 is identical in form to the classical Nernst–Planck equation. The major modification introduced here is that the potential function u includes ion–ion interaction terms and, therefore, is concentration dependent. The denominator ($h(\infty)$) in Eq. 1 is equivalent to the total resistance of the channel for ion i. Accordingly, $g(x)$ can be thought of as the contribution of the local resistance at x to the total (series) resistance.

The function (g) is plotted in Fig. 8 for an applied voltage of −100 mV, $N_2 = -2$, and $N_1 = -1.5$ and symmetrical solutions of either 150 or 300-mM monovalent ions. Large values of g correspond to the regions of the channel that limit the ion conductance. It can be seen from Fig. 2 that both the diffusion coefficient (D_i) and the cross-sectional area (A_i) are greatly reduced in the narrow region of the channel and this produces the two sharp peaks in $g(x)$ at the two ends of this narrow region. The large decrease in g near $X = 0$ results from the large negative value of u close to the fixed negative charge. The function $g(x)$ summarizes all the factors that influence ion movement and can be thought of as an equivalent energy barrier profile, such as is used in reaction-rate theory. In these terms, the g profile in Fig. 8 corresponds to the classical two barrier, one-site model. However, this general model differs fundamentally from the simple reaction-rate model because the shape of $g(x)$ (i.e., the energy profile) is not fixed, but changes as the concentration is changed as a result of the ion–ion interaction.

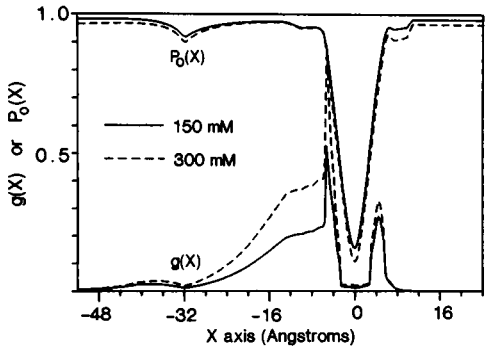

FIGURE 8 Profile of the general total channel resistance (g) in arbitrary units for pure symmetrical monovalent solutions of 150 or 300 mM. Also, profile of $P_o(X)$ (probability that no ion is in "one-ion region" $\sim X$). Applied voltage = −100 mV, $N_2 = -2$, $N_1 = -1.5$.

Also shown in Fig. 8 is a plot of $P_o(X)$, the probability that there are no ions in the "one-ion region" centered about X. As expected, the minimum value of P_o is found near the inner charged site ($X = 0$), reaching a value of 0.1, indicating that this region is occupied by an ion 90% of the time. As the fixed charge is increased, $P_o(0)$ decreases, reaching a value of $\sim 10^{-4}$ when N_1 is −2.5. The total potential energy can be written as (Levitt, 1990):

$$e^{z_i\gamma u_i} = \frac{1}{P_o} e^{z_i\gamma w_i}. \qquad (2)$$

The hard sphere repulsive potential factor corresponds to the $1/P_o$ term and w_i is the sum of all the other potential contributions. Thus, the small value of P_o at the ion charged site ($X = 0$) is associated with a large repulsive potential resulting from the ion–ion hard sphere repulsive potential. Despite this repulsive potential, the attractive potential from the fixed charge is so large that it dominates the total potential, producing the small value of g near $X = 0$.

The results in Fig. 8 indicate that the rate limiting locations for these relatively high concentrations are at the entrance and exit to the narrow charged site region. This is expected because at these high concentrations, the main resistance will be in the narrow region because of the reduced area and diffusion coefficient and because the hard sphere potential limits the number of ions that are allowed in this region.

Saturation

In the simple Nernst-Planck model, the conductance is directly proportional to the concentration, whereas experimentally, the conductance tends to saturate at high concentrations. One would hope that this more general

model could mimic this experimentally observed saturation. However, although the conductance versus concentration curves tend to level off (Figs. 3 and 4) they do not actually saturate and level off at some maximum value. As discussed previously (Levitt, 1990), one would expect saturation to occur when the "one-ion region" at the ion binding site ($X = 0$) becomes rate limiting. As seen in Fig. 8, this region is not rate limiting (because g is small) and thus the lack of saturation is not surprising. In an attempt to find saturation, the model was solved for the case where the diffusion coefficient was made very small (reduced by a factor of 1/20) in a narrow region (± 2 Å) around $X = 0$. Fig. 9 compares the profile of g with and without the addition of this modification. It can be seen that there is now an additional peak in g at $X = 0$, indiating that this region is now, at least, partially, rate limiting. Fig. 10 shows the corresponding conductance versus concentration curve. As predicted, there is now significantly greater saturation of the conductance.

This localized small diffusion coefficient can be thought of as mimicking the "binding" of an ion at a specific site. The above analysis suggests that those channels which show strong saturation should have this type of "binding" site.

COMPARISON WITH THE ACH RECEPTOR CHANNEL

The model calculations will be compared with two sets of experimental results: the investigation of Imoto et al. (1988) on *Torpedo* channel modified by site directed mutagenesis; and the studies of Dani and Eisenman (1987) on the rat myotube channel. Imoto et al. (1988) determined the I-V behavior in symmetrical 100 mM KCl and with the addition of 0.5 mM $MgCl_2$ to either side of the membrane. Dani and Eisenman (1987) measured I-V and conductance versus concentration curves for a variety of mixtures of monovalent and divalent ions.

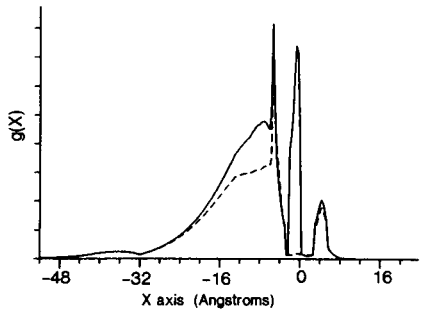

FIGURE 9 Profile of the general total resistance in symmetrical 150 mM monovalent with (——) or without (- - -) the diffusion coefficient reduced by a factor of 1/20 in a region of ±2 Å about $X = 0$. Applied voltage = −100 mV.

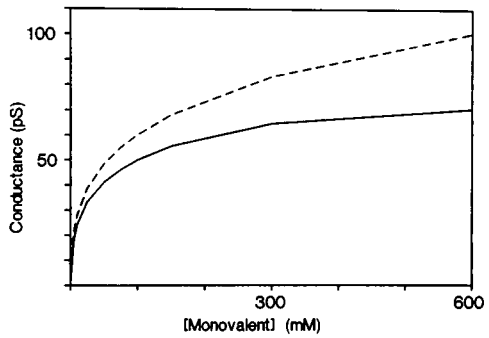

FIGURE 10 Conductance versus symmetrical monovalent concentration with (——) or without (- - -) the diffusion coefficient reduced by a factor of 1/20 in a region of ±2 Å about $X = 0$. Applied voltage = −100 mV.

Interaction between monovalent and divalent ions

If, as is assumed in the model, the interaction between the fixed charged site and the ion is purely electrostatic, then the only property of the ion that will influence its conductivity is its charge (assuming all ions have the same radius). Thus, one would expect that taking the ratio of the mono/divalent ion conductance should provide a direct probe of this electrostatic potential, with other factors in the model, such as the diffusion coefficient or physical pore area, canceling out of the ratio. One would like to be able to measure this ratio at ion concentrations where the charged site has the same fractional occupation by mono or divalent ions. However, because the divalent ions saturate the site at millimolar or lower concentrations where the conductance is too low to be measured, this is not experimentally practicable. An alternative approach that should provide information similar to that of the conductance ratio but that is experimentally feasible is to measure the fractional block of the monovalent conductance by the addition of divalents.

The rat and *Torpedo* ACH channels differ qualitatively in their interaction with divalents. For the *Torpedo* channel, the conductance in symmetrical 100 mM KCl is reduced by half by the addition of only 0.5 mM Mg^{++}, whereas in the rat, 1 mM Mg^{++} produces only a very small block (Dani and Eisenman, 1987), and 10 mM is required for a 50% block of the conductance in 150 mM

KCl (Decker and Dani, 1989). In the model calculations, the fractional block by divalents is very sensitive to the fixed charge in the narrow region (N_1). For example, in symmetrical 150 mM monovalent, when the fixed charge is increased from -1.3 (Fig. 6) to -2.3 (Fig. 7), the divalent concentration required for a 50% block falls from 16 to 0.35 mM. Extrapolating these model results to the ACH channel suggests that the *Torpedo* channel should have about one more negative charge than the rat channel at the narrow end. Consistent with this prediction, the *Torpedo* channel has one more negative charge at the inner end of the M2 segment, the putative ion binding site. (The gamma subunit of the mouse muscle (BC3H1) channel sequence (Patrick et al., 1987) has a positive lysine in place of the neutral glutamine in the *Torpedo* sequence (Imoto et al., 1988)).

The mutagenesis results of Imoto et al. (1988) are in qualitative, but not quantitative, agreement with the model predictions. For example, the model would predict that raising the net charge at the inner ring by +1 or +2 should make the block by 0.5 mM Mg^{++} so small that it could not be detected experimentally ($\sim 3\%$ or less). Imoto et al. (1988) find that, although the Mg^{++} block is reduced, it is still significant ($> 10\%$).

Monovalent ion conductance

As long as N_1 is -1 or more negative, the absolute value of the model conductance is in the same range (50–70 pS at 100 mM; Figs. 3 and 4) as the experimental conductance. This agreement is evidence that the model is, at least, consistent with the experimental data. The strength of this evidence is somewhat weakened by the fact that, although the parameters were chosen to be consistent with the known properties of the channel (shape and size dependence of ion conductance), they were also adjusted to give the desired absolute conductance values.

The model conductance increases monotonically as the net negative charge at the wide end of the channel is increased (Fig. 4). This charge dependence is in good quantitative agreement with the mutagenesis results of Imoto et al. (1988). In contrast, increasing the net negative charge at the narrow and (Fig. 3) can result in either an increase or decrease in model conductance. This does not agree with the observation of Imoto et al. (1988) of a large monotonic increase in conductance with increasing charge.

Current-voltage relationship

The model I-V curves are qualitatively similar to the experimental results for mouse and *Torpedo,* being relatively linear and having a larger conductance for currents in the inward direction. The curve at a fixed charge (N_1) of -1 is more asymmetrical than the experimental result whereas the curve for $N_1 = -2$ is quite close to the experimental result. The model I-V curves with divalent added to the external solution are also similar to the experimental results, with the block being relieved at large positive potentials.

Conductance versus concentration

The experimental results on the rat channel are qualitatively similar to the model results, with a relatively high conductance at low concentrations resulting from the negative fixed charges and a tendency to level off and saturate at high concentrations. As noted above, the model curves do not actually saturate because the conductance increases steadily by $\sim 20\%$ for a doubling of the concentration over the concentration range of 150–600 mM. This model result agrees quantitatively with the experimental data for Na^+ (Dani and Eisenman, 1987). In contrast, their experimental data for Cs^+ are more suggestive of a true saturation, and, therefore, cannot be fit by the standard model. As discussed above, to get this type of saturation in the model it is necessary to modify the model by using a very small diffusion coefficient in a localized region at the charged site, mimicking specific ion "binding".

Comparison with NMDA channel

The *N*-methyl-*D*-aspartate (NMDA) channel is thought to be structurally similar to the ACH channel and has similar monovalent ion conductance. However, there is one property of the NMDA channel that differs dramatically from that of ACH. In the ACH channel, Ca^{++} and Mg^{++} have similar conductances. In contrast, the NMDA channel has a relatively high Ca^{++} conductance, whereas Mg^{++} is a very potent voltage dependent channel blocker (Ascher and Nowak, 1988). The model presented here can be used to address the question of how the ACH channel would have to be modified to explain this different behavior. The simplest possibility would be if there was a small change at the narrow fixed charge site which prevented the more tightly hydrated Mg^{++} from passing through the channel (e.g., a slight decrease in diameter), with all other properties of the channel (fixed charges, etc.) remaining unchanged.

This blocking condition can be easily incorporated into the model solution by setting the Mg^{++} flux equal to zero with the Mg^{++} ions that are on the left (right) side of the binding site in equilibrium with the left (right)

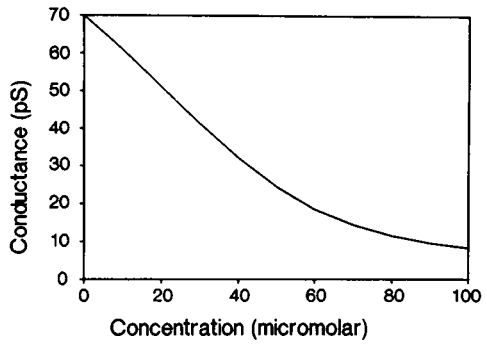

FIGURE 11 Conductance versus divalent cation conductance for channel conditions that are identical to those in Fig. 6 except that the divalent cannot get past the narrow binding site region. These conditions may mimic those of the NMDA channel.

bulk solution. The conductance versus Mg^{++} concentration is shown in Fig. 11 for this "divalent blocked" condition for a channel that is otherwise identical to that used in Fig. 6 (applied voltage of 100 mV, inside negative; $N_1 = -1.3$; 150 mM symmetrical monovalent). For the ACH channel, addition of the divalent ion produced a slight decrease in conductance, reducing the flux by half at a concentration of ~15 mM. In contrast, imposing the condition that the divalent cannot get past the binding site (while using an identical channel model), lowered the half maximal blocking concentration to ~37 μM. This blocking affinity is close to that observed experimentally for the NMDA channel (72 μM at −60 mV). This result demonstrates that only a very small modification of the ACH channel is required to convert it to a channel with properties characteristic of the NMDA channel.

The case where the divalent cannot get past the binding site (NMDA channel) is exactly equivalent to assuming that the divalent ion on either side of the binding site is at equilibrium. I was surprised that the divalent channel block was so effectively relieved simply by relaxing this "equilibrium" assumption and allowing the divalent ion to pass through the site (without any other change in the model).

I find this prediction of the model particularly convincing, because it was looked for as an afterthought, after all the parameters had been chosen for the ACH channel. It illustrates what I believe should be the main application of this model, which is to investigate qualitative channel features. There are so many adjustable (and unknown) parameters in the model that it is probably not useful to try and fit the detailed quantitative features of the channel kinetics.

CONCLUSIONS

The model of the channel presented here requires only two sets of information about the channel, its geometric shape and the location and magnitude of the fixed charges. (Other features of the model, such as the electrostatic cross-sectional area or the diffusion coefficient in the channel can be estimated given the channel geometry.) The flux of all the ions that are present can then be directly determined from these channel properties without any additional assumptions. This is a major advantage of the model because this level of information is at (or beyond) the limit of what can be inferred about the actual channel at the present time.

The channel parameters used in these calculations were only roughly adjusted in an attempt to fit the main qualitative features of the ACH channel, and no attempt was made to fine tune them to optimize the fit. The model calculations are in qualitative, and in some cases, quantitative agreement with most of the experimental data that is available for the ACH channel. The model has the correct absolute conductance and I-V curve. The low affinity Mg^{++} block of the rat muscle ACH channel and the high-affinity block of the *Torpedo* ACH channel can be fit by a fixed charge at the narrow end of −1.3 (rat) or −2.3 (*Torpedo*) and this charge difference is consistent with the differences in the amino acid sequence of the two species. The conductance versus concentration curve of the model is similar to the experimental results for Na^+, but the model cannot fit the experimental data for Cs^+. The model must be modified by the addition of a "specific binding" at the fixed charge site to fit the experimental Cs^+ data.

One would expect that the site-directed mutagenesis experiments of Imoto et al. (1988) in which the charges at the two ends of the channel are systematically varied should provide the strictest test of the model. The model calculations are quantitatively consistent with the experimental variations of charge at the wide end of the channel. However, the model predictions of the variation in monovalent conductance or divalent block with alterations in charge at the narrow end differ significantly from the experimental results. This may indicate a limitation of the model. Alternatively, it may suggest that experimental variations in charge at the narrow end are also associated with some additional structural changes in the channel. This would not be surprising considering the large electrostatic forces that should be associated with these charges.

APPENDIX

Electrostatic and physical cross-sectional area

The following dimensionless parameters are used: x, l, r_2, t_1, t_2, g_1, and g_2 are equal to X, L, R_2, T_1, T_2, G_1, and G_2 divided (normalized) by R_1 (see Fig. 1 for a definition of these parameters). The dimensionless electrostatic area is defined by $a_e = A_e/(2\pi R_1^2)$. To simplify the equations, the expression for the electrostatic area is modified slightly from previous derivations (Levitt, 1985, 1987). At each x, a_e is defined in terms of an effective hemispherical surface:

$$\begin{aligned} a_e &= x^2 \qquad 1 < x \\ &= 1 \qquad -1-g_2 < x < 1 \\ &= y^2 \qquad \ell - r_2 < x < -1-g_2 \\ &= (x+\ell)^2 \qquad x < -\ell - r_2 \end{aligned}$$

$$y = \frac{(1-r_2)x + \ell - r_2 g_2}{(\ell - r_2 - 1 - g_2)}. \tag{1A}$$

The solid lines in Fig. 12 show this area.

The physical cross-sectional area for the ith ion (a_i) is the area available to the center of the ion. The large dashed lines in Fig. 12 represent the physical surface of the channel. The center of the ion can then approach to within one ion radius of this surface, indicated by the short dashed lines. The corresponding area is described by:

$$\begin{aligned} a_i &= (x-g_1)(x-g-\beta) \qquad t_1 + g_1 < x \\ &= 0.5[(t_1-\beta)^2 + (x-g_1)^2(1-\beta^2/t_1^2)] \qquad -g_1 < x < t_1 + g_1 \\ &= 0.5(t_1-\beta)^2 \qquad -g_2 < x < g_1 \\ &= 0.5(z-\beta)^2 \qquad -\ell < x < -g_2 \\ &= 0.5[(t_2-\beta)^2 + (x+\ell)^2(1-\beta^2/t_2^2)] \qquad -\ell - t_2 < x < -\ell \\ &= (x+\ell)(x+\ell+\beta) \qquad x < -\ell - t_2 \end{aligned}$$

$$z = (x+g_2)\left(\frac{t_1-t_2}{\ell-g_2}\right) + t_1. \tag{2A}$$

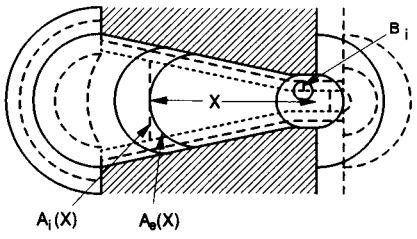

FIGURE 12 Scale drawing of channel showing electrostatic area (A_e, — —, Eq. 1A) and restricted physical area available to ion of radius B_i (A_i, - - -, Eq. 2A) at different axial (X) positions. The long dashed line shows the physical dimensions of the channel. The region of the channel accessible to the ion (*short dashes*) is equal to the physical radius minus the ion radius.

Electrostatic potential

The derivation has been described previously (Levitt, 1985, 1987). The central function is $E(x, x_o)$, the E field at x from a charge ne at x_o. It is used to determine both the ion–wall and ion–ion interaction potential.

$$\begin{aligned} \xi(x, x_o) &= \epsilon_w R_1^2 E/e = n[\alpha(x_o) \pm 1]/a_e(x) \\ \alpha(x_o) &= [1 - 2I(x_o)/I(-\infty)] \\ I(x_o) &= I_1(x_o) + I_2(-\ell - r_2) + I_3(-1-g_2) \\ &\quad + I_4(1) \qquad x_o < -\ell - r_2 \\ &= I_2(x_o) + I_3(-1-g_2) \\ &\quad + I_4(1) \qquad -\ell - r_2 < x_o < -1 - g_2 \\ &= I_3(x_0) + I_4(1) \qquad -1 - g_2 < x_o < 1 \\ &= I_4(x_o) \qquad 1 < x_o \\ I_1(x) &= 1/r_2 + 1/(x+\ell) \\ I_2(x) &= \frac{(1+g_2-\ell-g_2)(1+g_2+x)}{(1-r_2)x + \ell - r_2 g_2} \\ I_3(x) &= 1 - x \qquad I_4(x) = 1/x. \end{aligned} \tag{3A}$$

The + or − in the definition of E corresponds to x greater than or less than x_o, respectively.

The Born image potential energy U_B for an ion of charge ne at x is described by (see Levitt, 1987):

$$\begin{aligned} u_B(x) &= \epsilon_w R_1^2 U_B/e^2 \\ &= 0.5n^2[(\alpha(x)+1)I(x) - 2/y(x)] \qquad -\ell < x < 0 \\ &= u_B(-\ell) f(x)/f(-\ell) \qquad x < -\ell \\ &= u_B(0) f(x/f(0) \qquad 0 < x \\ f(x) &= [\alpha(x)+1]I(x) \\ y &= \text{electrostatic radius at } x. \end{aligned} \tag{4A}$$

The expressions for $x < -\ell$ and $x > 0$ are empirical extrapolations.

The applied voltage profile $V(x)$ is described by:

$$v = \epsilon_w R_1 V/e = v_2 + (v_1 - v_2)I(x)/I(-\infty), \tag{5A}$$

where v_1 and v_2 are the dimensionless voltages on the two sides of the membrane.

Definition of "one-ion region"

The "one-ion region" at x_o is the region about x_o in which there can be at most one ion. For x_o within or near the narrow region, the one-ion region is defined as all the ions within the following range of x.

$$\begin{aligned} -g_2 - 3r_{HS} < x < x_o + r_{HS} &\text{ for } -g_2 - 3r_{HS} < x_0 < -g_2 - 2r_{HS} \\ x_o - r_{HS} < x < x_o + r_{HS} &\text{ for } -g_2 - 2r_{HS} < x_o < g_1 + r_{HS} \\ x_o - r_{HS} < x < g_1 + 2r_{HS} &\text{ for } g_1 + r_{HS} < x_o < g_1 + 2r_{HS}. \end{aligned}$$

The concentration of ions in this region is summed exactly. For x_o external to this region, the one-ion region is defined as equal to the number of ions in a volume equal to a sphere of radius r_{HS} with an average concentration equal to the concentration at x_o.

Diffusion coefficient in channel

The diffusion coefficient at x in the channel relative to the bulk diffusion coefficient ($D(x)/D_o$) is assumed to be equal to the continuum expression for a sphere of radius b (the ion radius) in an infinite uniform cylinder of radius $w(x)$, the radius of the channel at x ($=b/w$; Levitt, 1975):

$$\frac{D(x)}{D_o} = \frac{1 - 2.1054\lambda + 2.0805\lambda^3 - 1.7068\lambda^5 + 0.72603\lambda^6}{1 - 0.75857\lambda^5}. \quad (6A)$$

I wish to thank John Dani and Rad Decker for their helpful suggestions and for sending me their unpublished data.

Received for publication 4 December 1989 and in final form 15 October 1990.

REFERENCES

Ascher, P., and L. Nowak. 1988. The role of divalent cat ions in *N*-methyl-D-aspartate responses of mouse central neurons in culture. *J. Physiol. (Lond.)*. 399:247–266.

Dani, J. A. 1989*a*. Open channel structure and ion binding sites of the nicotinic acetylcholine receptor channel. *J. Neurosci.* 9:882–890.

Dani, J. A. 1989*b*. Site-directed mutagenesis and single-channel currents define the ionic channel of the nicotinic acetylcholine receptor. *TINS (Trends Neurosci.)* 12:125–128.

Dani, J. A., and G. Eisenman. 1987. Monovalent and divalent cation permeation in acetylcholine receptor channels: ion transport related to structure. *J. Gen. Physiol.* 89:959–983.

Decker, E. R., and J. A. Dani. 1989. Calcium permeability of the nicotinic acetylcholine receptor channel determined from single-channel measurements in BC3H1 cells. *Biophys. J.* 551a. (Abstr.)

Eisenman, G., A. Villarroel, M. Montal, and O. Alvarez. 1990. Energy profiles for ion permeation in pentameric protein channels: from viruses to receptor channels. *In* 13th International Conference on Biological Membranes. Control of Membrane Function: Short-Term and Long Term. P. J. Magistretti and J. M. Ritchie, editors. Alan R. Liss, Inc. New York.

Furois-Corbin, S., and A. Pullman. 1988. Theoretical study of potential ion-channels formed by bundles of α-helices. Partial modeling of the acetylcholine receptor channel. *In* Transport through Membranes: Carriers, Channels and Pumps. A. Pullman et al. editors. Kluwer Academic Publishers Group, Dordrect, The Netherlands. pp. 337–357.

Hille, B. 1984. *Ionic Channels of Excitable Membranes.* Sinauer Associates Inc., Sunderland, MA. 241–247.

Imoto, K., C. Busch, B. Sakmann, M. Mishina, T. Konno, J. Nakai, H. Bujo, Y. Mori, K. Fukuda, and S. Numa. 1988. Rings of negatively charged amino acids determine the acetylcholine receptor channel conductance. *Nature (Lond.)*. 335:645–648.

Levitt, D. G. 1975. General continuum analysis of transport through pores. I. Proof of Onsager's reciprocity postulate for uniform pore. *Biophys. J.* 15:533–551.

Levitt, D. G. 1985. Strong electrolyte continuum theory solution for equilibrium profiles, diffusion limitation, and conductance in charged ion channels. *Biophys. J.* 48:19–31.

Levitt, D. G. 1987. Exact continuum solution for a channel that can be occupied by two ions. *Biophys. J.* 52:455–466.

Levitt, D. G. 1990. General continuum theory for multi-ion channel. I. Theory. *Biophys. J.* 59:271–277.

Patrick, J., J. Boulter, D. Goldman, P. Gardner, and S. Heinemann. 1987. Molecular biology of nicotinic acetylcholine receptors. *Ann. NY. Acad. Sci.* 505:194–207.